AGU PUBLICATIONS

JGR

Journal of Geophysical Research: Atmospheres

RESEARCH ARTICLE
10.1002/2014JD022394

Key Points:
- Bayesian inversion estimates of methane emissions in East Asia
- Methane emissions from China increased by 3% annually from 2000 to 2011
- China contributes significantly to the increase in global methane emissions

Correspondence to:
R. L. Thompson,
rlt@nilu.no

Citation:
Thompson, R. L., et al. (2015), Methane emissions in East Asia for 2000–2011 estimated using an atmospheric Bayesian inversion, *J. Geophys. Res. Atmos.*, *120*, 4352–4369, doi:10.1002/2014JD022394.

Received 4 AUG 2014
Accepted 26 MAR 2015
Accepted article online 28 MAR 2015
Published online 5 MAY 2015

Methane emissions in East Asia for 2000–2011 estimated using an atmospheric Bayesian inversion

R. L. Thompson[1], A. Stohl[1], L. X. Zhou[2], E. Dlugokencky[3], Y. Fukuyama[4], Y. Tohjima[5], S.-Y. Kim[6], H. Lee[7], E. G. Nisbet[8], R. E. Fisher[8], D. Lowry[8], R. F. Weiss[9], R. G. Prinn[10], S. O'Doherty[11], D. Young[11], and J. W. C. White[12]

[1]Norwegian Institute for Air Research, Kjeller, Norway, [2]Chinese Academy of Meteorological Sciences, Beijing, China, [3]Global Monitoring Division, National Oceanic and Atmospheric Administration, Boulder, Colorado, USA, [4]Japan Meteorological Agency, Tokyo, Japan, [5]National Institute for Environmental Studies, Tsukuba, Japan, [6]National Institute of Environmental Research, Incheon, South Korea, [7]Korea Meteorological Administration, Seoul, South Korea, [8]Department of Earth Sciences, Royal Holloway University of London, London, UK, [9]Scripps Institution of Oceanography, University of California, San Diego, La Jolla, California, USA, [10]Massachusetts Institute of Technology, Cambridge, Massachusetts, USA, [11]Atmospheric Chemistry Research Group, School of Chemistry, University of Bristol, Bristol, UK, [12]Institute of Arctic and Alpine Research, University of Colorado, Boulder, Colorado, USA

Abstract We present methane (CH_4) emissions for East Asia from a Bayesian inversion of CH_4 mole fraction and stable isotope ($\delta^{13}C$-CH_4) measurements. Emissions were estimated at monthly resolution from 2000 to 2011. A posteriori, the total emission for East Asia increased from 43 ± 4 to 59 ± 4 Tg yr^{-1} between 2000 and 2011, owing largely to the increase in emissions from China, from 39 ± 4 to 54 ± 4 Tg yr^{-1}, while emissions in other East Asian countries remained relatively stable. For China, South Korea, and Japan, the total emissions were smaller than the prior estimates (i.e., Emission Database for Global Atmospheric Research 4.2 FT2010 for anthropogenic emissions) by an average of 29%, 20%, and 23%, respectively. For Mongolia, Taiwan, and North Korea, the total emission was less than 2 Tg yr^{-1} and was not significantly different from the prior. The largest reductions in emissions, compared to the prior, occurred in summer in regions important for rice agriculture suggesting that this source is overestimated in the prior. Furthermore, an analysis of the isotope data suggests that the prior underestimates emissions from landfills and ruminant animals for winter 2010 to spring 2011 (no data available for other times). The inversion also found a lower average emission trend for China, 1.2 Tg yr^{-1} compared to 2.8 Tg yr^{-1} in the prior. This trend was not constant, however, and increased significantly after 2005, up to 2.0 Tg yr^{-1}. Overall, the changes in emissions from China explain up to 40% of the increase in global emissions in the 2000s.

1. Introduction

Methane (CH_4) is an important greenhouse gas (GHG) contributing 0.48 Wm^{-2} to radiative forcing [*Myhre et al.*, 2013]. In recent years, CH_4 has been discussed as an appealing target for global warming mitigation strategies. This is because CH_4 has a relatively short atmospheric lifetime, ~10 years, which means that reducing CH_4 emissions would result in reductions in radiative forcing after only a few years. Furthermore, CH_4 has a much larger global warming potential (GWP) than CO_2 (a GWP of 28 on a 100 year time horizon), meaning that for an equal mass emission of CH_4 and CO_2, CH_4 contributes much more to radiative forcing than CO_2 [*Myhre et al.*, 2013].

The budget of CH_4 was close to steady state in the early 2000s, with the sum of emissions being almost balanced by the sum of the sinks, that is oxidation by the OH radical in the troposphere and, to a lesser extent, reaction with chlorine radicals in the marine boundary layer and with $O(^1D)$, OH, and photodissociation in the stratosphere, as well as a small but significant sink via oxidation by methanotrophic bacteria in soils [*Ridgwell et al.*, 1999]. The main sources of CH_4 emissions can be divided into natural (wetlands, geological seeps, termites, methane hydrates, and oceans) and anthropogenic sources (coal, oil and gas exploitation, rice cultivation, domestic ruminant animals, and waste) [*Kirschke et al.*, 2013]. From the mid-1990s to the mid-2000s, the atmospheric growth rate of CH_4 was close to zero, reflecting the near balance of its sources and sinks. However, since 2006, the growth rate has become positive again [*Dlugokencky et al.*, 2011; *Nisbet et al.*, 2014; *Rigby et al.*, 2008]. The reason for this increase is

still not fully understood but is likely due to a combination of increased anthropogenic emissions as well as an increase in tropical and subtropical wetland emissions driven by climate variability [*Kirschke et al*., 2013]. Larger anthropogenic emissions are likely due to an expansion of oil, gas, and coal exploitation, which has been driven at least in part by economic growth in East Asia and, especially, China, where coal production alone rose on average 10%/yr between 2000 and 2009 [*Cheng et al*., 2011].

China is the world's largest developing country and has come under recent focus for policy makers and researchers, as it is, since 2007, the world's largest emitter of CO_2 [*Gregg et al*., 2008]. Methane makes up a substantial part of China's total GHG emissions, accounting for an estimated 23% of the emissions by CO_2 equivalency using GWP [*Zhang and Chen*, 2010]. China's CH_4 sources are largely agriculture, particularly rice cultivation and coal mining. While emissions from rice cultivation are thought to have declined [*Chen et al*., 2013], those related to coal have increased substantially over the past decade [*Cheng et al*., 2011]. However, bottom-up estimates of CH_4 emissions for East Asia differ considerably. For instance, those for Chinese coal mining differ by almost 200% for a single year [*Cheng et al*., 2011; *Zhang and Chen*, 2010]. Bottom-up emission estimates can be constrained using atmospheric CH_4 mole fraction measurements, that is using the top-down approach [*Weiss and Prinn*, 2011]. For East Asia, specifically, emissions have been approximated using measured atmospheric CH_4 to CO_2 ratios [*Tohjima et al*., 2014] and the radon tracer method [*Wada et al*., 2013]. Although these methods provide an estimate of the total emission and its temporal variability, information about the spatial distribution and the source of the emissions is limited. Another top-down method is atmospheric inversion, which uses an atmospheric transport model to relate changes in mole fractions to emissions and optimizes the emissions in a statistically rigorous way. Inversion estimates for CH_4 emissions in East Asia have been hitherto based only on global scale studies [e.g., *Bergamaschi et al*., 2009, 2013; *Chen and Prinn*, 2006; *Mikaloff Fletcher et al*., 2004] and, thus, provide information only at coarse spatial resolution.

In this study, we estimate total CH_4 emissions in East Asia using atmospheric observations of CH_4 mole fractions in a Bayesian inversion. Emissions are estimated monthly from 2000 to 2011 and over the domain from 70°E to 150°E and 10°N to 55°N. Atmospheric transport is modeled using the Lagrangian Particle Dispersion Model (LPDM), FLEXible PARTicle dispersion model (FLEXPART) [*Stohl et al*., 1998, 2005], and the inversion framework, FLEXINVERT, developed by *Thompson and Stohl* [2014]. LPDMs represent an advantage in atmospheric tracer transport over Eulerian models, as they can have quasi-infinite resolution and they are not subject to numerical diffusion, which in Eulerian models can lead to "smearing" of the calculated fields of concentrations and/or source-receptor relationships (SRRs). (In this paper, SRRs refer to the relationship between sensitivity of a "receptor" element or observation, *y*, to a "source" element, *x*, following *Seibert and Frank* [2004].) The emissions are solved on a grid of varying resolution, which has been optimized based on the SRRs to give maximum resolution ($1.0° \times 1.0°$) in regions where there is strong contribution from emissions to the change in CH_4 mole fractions and minimum resolution ($8.0° \times 8.0°$) where there is only weak contribution, following the method of *Stohl et al.* [2010]. In this way, we can achieve a much higher spatial resolution where there is a good constraint from atmospheric observations, and aggregating grid cells only where there is a weak constraint does not significantly increase the aggregation error.

In this paper, we first outline the Bayesian inversion method as well as provide details about the prior information and observations used. Second, we present the results for the total CH_4 emissions using measurements of CH_4 mole fractions and the results from an inversion of CH_4 stable isotope fractions to estimate the emissions from different source types. Lastly, we discuss these results in comparison to independent estimates.

2. Methodology

2.1. Bayesian Inversion

We employ the Bayesian inversion framework, FLEXINVERT, which has been recently developed by *Thompson and Stohl* [2014]. FLEXINVERT is based on SRRs calculated by the LPDM and FLEXPART. Since the transport is a linear operation in this case and since it can be defined by a matrix operator, the problem is solved analytically. This can be represented by equation (1), where $\mathbf{y}^{\mathbf{obs}}$ is the observation vector (i.e., CH_4 mole

fractions measured at several sites), **x** is the state vector (i.e., CH_4 surface fluxes), **H** is the transport operator, and ε is the model and observation error.

$$\mathbf{y^{obs}} = \mathbf{Hx} + \varepsilon \tag{1}$$

Since the LPDM only accounts for transport backward in time over a few days, the history of the air mass previous to this (the so-called background) needs to be accounted for in $\mathbf{y^{obs}}$ or **H** (the background definition is discussed in detail in section 2.7). It is not possible to solve equation (1) for the state vector, **x**, because **H** is ill-conditioned and has no unique inverse. Bayes' theorem offers a method for determining **x** by regularizing the problem using prior information, i.e., a prior estimate of the fluxes. In this way, the posterior distribution of the fluxes can be found from the distribution of the observations and the prior fluxes leading to the cost function in equation (2) (for a full description of Bayesian inversion refer to, e.g., *Tarantola* [2005]).

$$J(\mathbf{x}) = \frac{1}{2}(\mathbf{x}-\mathbf{x_b})^T\mathbf{B}^{-1}(\mathbf{x}-\mathbf{x_b}) + \frac{1}{2}\left(\mathbf{Hx}-\mathbf{y^{obs}}\right)^T\mathbf{R}^{-1}\left(\mathbf{Hx}-\mathbf{y^{obs}}\right) \tag{2}$$

where $\mathbf{x_b}$ is the prior state vector, **B** is the prior error covariance matrix, and **R** is the observation error covariance matrix. The observation error also contains the model errors that are not related to the surface fluxes. Minimizing equation (2), the following equation can be derived for the optimal state vector, **x**:

$$\mathbf{x} = \mathbf{x_b} + \mathbf{BH}^T\left(\mathbf{HBH}^T + \mathbf{R}\right)^{-1}\left(\mathbf{y^{obs}} - \mathbf{Hx_b}\right) \tag{3}$$

In this study, the state vector contains the monthly unknown surface fluxes on the grid of variable resolution (see Figure 1) and has resolution of between 1.0° × 1.0° and 8.0° × 8.0° (for a full description of how the grid is defined, refer to *Thompson and Stohl* [2014] and *Stohl et al.* [2010]). For each month, the number of flux variables to be solved was 1276. The posterior error covariance matrix, **A**, is equivalent to the inverse of the second derivative of the cost function.

Since negative values for the fluxes are within the range of probability but are physically unlikely (the soil sink is expected to be close to negligible for the region of interest), we applied a subsequent inequality constraint on the fluxes following the method of *Thacker* [2007]. This is a truncated Gaussian approach in which inequality constraints are applied as error-free "observations":

$$\hat{\mathbf{x}} = \mathbf{x} + \mathbf{AP}^{\mathsf{T}}\left(\mathbf{PAP}^{\mathsf{T}}\right)^{-1}(\mathbf{c} - \mathbf{Px}) \tag{4}$$

where **A** is the posterior error covariance matrix, **P** is a matrix operator to select the variables that violate the inequality constraint, and **c** is a vector of the inequality constraint, which in this case is zero. The influence of this constraint is discussed in section 3.1.

2.2. Estimation of the Contribution From Different CH_4 Source Types

The Bayesian inversion method described in section 2.1 was adapted to estimate the contribution from different source types to the total CH_4 emission from China. For this, we use measurements of atmospheric CH_4 mole fractions and methane stable isotope ratios (written as δ^{13}C-CH_4). The δ^{13}C-CH_4 is the fractional deviation of the isotopic ratio of a sample from a standard and is expressed in units of per mil (‰). One can write an equation for the CH_4 sources in terms of CH_4 and δ^{13}C-CH_4 [*Mikaloff Fletcher et al.*, 2004]:

$$\delta_j^{\mathrm{obs}} y_j^{\mathrm{obs}} - \delta_j^{\mathrm{bg}} y_j^{\mathrm{bg}} = \sum_{i=1}^{N} H_{ji}\delta_i^{\mathrm{src}} x_i \tag{5}$$

where δ_j^{obs} and y_j^{obs} are, respectively, the δ^{13}C-CH_4 and CH_4 mole fractions of the *j*th observation and δ_j^{bg} and y_j^{bg} are, respectively, the δ^{13}C-CH_4 and CH_4 mole fractions of the background for the *j*th observation. H_{ji} is the source-receptor relationship for the *j*th observation and the *i*th source, and δ_i^{src} and x_i are, respectively, the δ^{13}C-CH_4 and the magnitude of the source. We calculate the change in δ^{13}C-CH_4 and CH_4 mole fractions from Chinese emissions and compare these in the Bayesian inversion framework with the observations to optimize the emissions by source type. The state vector in this case is a vector of scalars for $N = 7$ different source types in China. For the prior values of the scalars, we used a vector of ones, and we assumed an uncertainty of 10%. (This is approximately half the uncertainty of the total source in the domain. Since the true uncertainty of the different sources is unknown, we considered a value that was smaller than the total uncertainty of all sources to be appropriate.) We chose to restrict the inversion to

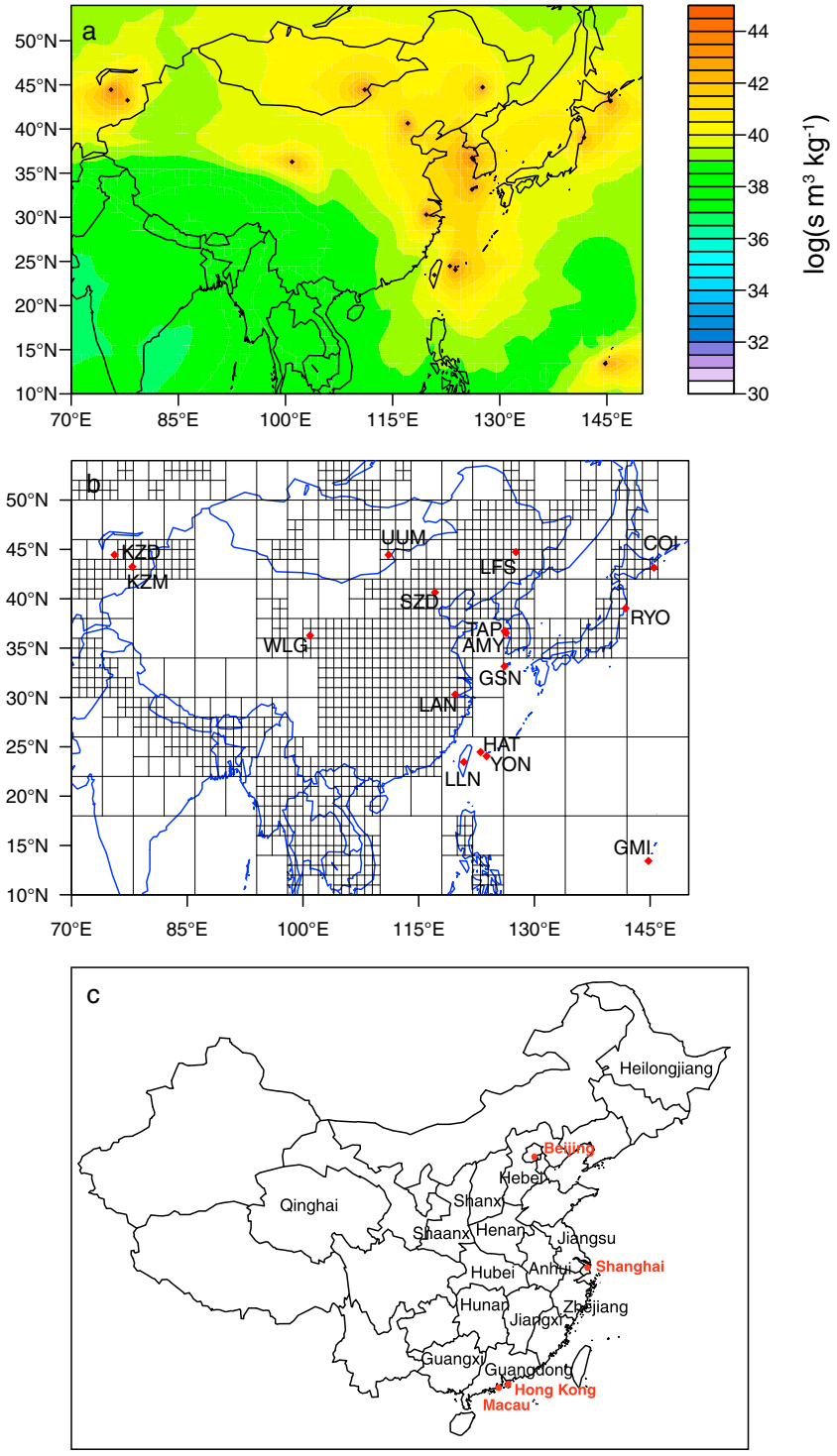

Figure 1. Sensitivity to the surface emissions (i.e., the footprint or equivalently source-receptor relationship) integrated over all observation sites and all time steps for the year 2009 (units of log(s m^3 kg^{-1})). (a) The black dots indicate the site locations. (b) Variable grid used in the inversion also showing the location of the observation sites (red dots). (c) Map of China illustrating the provinces and cities that are mentioned in this study.

seven source categories as the amount of information provided from the few observations is limited, and furthermore, we found that using larger numbers of source categories prevented the algorithm from converging. Since the time period of the observations is also short (December 2010 to April 2011), we

calculate only the mean emissions over this time period, i.e., winter to spring. Given the limited data available, we present this estimation of the source types using δ^{13}C-CH_4 only as a "proof of concept."

2.3. Atmospheric Transport

The SRRs were calculated using the backward mode of FLEXPART, in which virtual particles are followed backward in time from the observation sites (or receptors). This is more efficient than forward calculations as the number of observation sites is smaller than the number of unknown flux grid cells. Furthermore, particle releases in the backward mode can be made exactly at the measurement point, which avoids initial diffusion of information into a grid cell. This is an important advantage of LPDMs, which facilitate high spatial resolution of the model output around the measurement sites. FLEXPART simulations were made using European Centre for Medium-Range Weather Forecasts ERA-Interim meteorological analyses, and retroplumes were calculated at 3-hourly intervals at each of the receptors. We released 10,000 particles for each retroplume, which were followed backward in time for 20 days. Given the atmospheric lifetime of CH_4 (approximately 10 years), the oxidative loss of CH_4 during such a short period is not substantial; however, it was accounted for using monthly climatological OH fields taken from the atmospheric chemistry transport model, Goddard Earth Observing System-Chemistry model (http://acmg.seas.harvard.edu/geos/). For computational efficiency, the inversions were performed for each year in parallel (i.e., using 12 month windows) over the period from 2000 to 2011.

2.4. Atmospheric Mole Fractions

Atmospheric observations of CH_4 dry-air mole fractions (units of nmol mol^{-1}, abbreviated as ppb) were pooled from four networks plus a number of independent sites (for the full list, see Table 1). In the East Asian domain, 16 sites were included with 16 additional sites outside the domain. Of the additional sites, those that are downstream of the domain provide some constraint on the fluxes inside the domain, while the other sites were included only as a check on the background calculation and had negligible impact on the fluxes found in the inversion (the background calculation is described in section 2.7). We include approximately weekly data from discrete flask samples from the National Oceanic and Atmospheric Administration Carbon Cycle and Greenhouse Gases (NOAA CCGG) network, which are measured using a gas chromatograph fitted with a flame ionization detector (GC-FID) and reported on the NOAA-X2004 scale [*Dlugokencky et al.*, 2005]. Additionally, we include approximately hourly data from the Advanced Global Atmospheric Gases Experiment (AGAGE), which are made using in situ GC-FID and are reported on the Tohoku University scale [*Cunnold et al.*, 2002]. In East Asia, we use approximately hourly data from the National Institute for Environmental Sciences (NIES) and Japanese Meteorological Agency (JMA) networks, which are also made using in situ GC-FID and are reported on the NIES and NOAA-X2004 scales, respectively. In 2009, four new in situ sites were established by the Chinese Academy of Meteorological Sciences (CAMS). Measurements at these sites are made using Cavity ring-down spectroscopy and are reported approximately hourly on the NOAA-X2004 scale [*Fang et al.*, 2013]. These data were only available to us for 2009. A further two independent sites were included, Anmyeon-do and Gosan, both using in situ GC-FID. Anmyeon-do is operated by the Korean Meteorological Administration (KMA) and uses the Korea Research Institute of Standards and Science scale, and Gosan is operated by the Korean National Institute of Environmental Research (NIER) and uses the NOAA-X2004 scale.

The calibrations of all these stations and networks were compared using the results of intercomparisons of NOAA gas standards (http://www.esrl.noaa.gov/gmd/ccgg/wmorr/). The regression coefficients (and intercepts) for the given station/network compared to the NOAA-X2004 scale at NOAA were KMA = 0.9998 (32.8 ppb), NIES = 1.0087 (−12.3 ppb), JMA = 0.9998 (0.6 ppb), and CAMS = 1.0085 (−15.5 ppb). The Tohoku University scale (used by AGAGE) is nondistinguishable from the NOAA-X2004 scale at NOAA, so no correction was made to the AGAGE data.

All data were filtered for suspicious values using the flagging given by the data providers. In addition, the data were filtered for outliers, which were defined as values outside 2 standard deviations of the running mean using 90 days for flask and 3 days for in situ data. For the flask data, at most sites, no data were discarded; however, in a few cases, up to 6% of the data were discarded, including both data below and above 2 standard deviations around the running mean. For the in situ data, less than 4% of the data were discarded at each site. The flask data were then used in the inversion with no further filtering or averaging.

Table 1. Observation Sites Included in the Inversion (FM = Flask Measurement, IM = In Situ Measurement)[a]

Site ID	Organization	Latitude	Longitude	Altitude	Period	Type	Description
ALT	NOAA	82.5°N	62.5°W	205	2000–2011	FM	Alert, Nunavut, Canada
SUM	NOAA	72.6°N	38.5°W	3238	2000–2011	FM	Summit, Greenland
CBA	NOAA	55.2°N	162.7°W	25	2000–2011	FM	Cold Bay, Alaska
MHD	AGAGE	53.3°N	9.9°W	25	2000–2011	IM	Mace Head, Ireland
SHM	NOAA	52.7°N	174.1°E	40	2000–2011	FM	Shemya Island, Alaska
LFS	CAMS	44.7°N	127.6°E	331	2009	IM	Longfengshan, China
UUM	NOAA	44.5°N	111.1°E	914	2000–2011	FM	Ulaan Uul, Mongolia
KZD	NOAA	44.5°N	75.6°E	412	2000–2010	FM	Sary Taukum, Kazakhstan
KZM	NOAA	43.3°N	77.9°E	2519	2000–2010	FM	Plateau Assy, Kazakhstan
COI	NIES	43.2°N	145.5°E	45	2000–2011	IM	Cape Ochi-ishi, Japan
THD	AGAGE	41.1°N	124.2°W	107	2000–2011	IM	Trinidad Head, USA
SDZ	CAMS/NOAA	40.7°N	117.1°E	293	2009[b]	IM/FM	Shangdianzi, China
RYO	JMA	39.0°N	141.8°E	260	2000–2011	IM	Ryori, Japan
AZR	NOAA	38.8°N	27.1°W	30	2000–2011	FM	Azores
TAP	NOAA	36.7°N	126.1°E	20	2000–2011	FM	Tae-ahn Penninsula, South Korea
AMY	KMA	36.5°N	126.3°E	47	2007–2011	IM	Anmyeon-do, South Korea
WLG	CAMS/NOAA	36.3°N	100.9°E	3816	2009[c]	IM/FM	Mt Waliguan, China
GSN	NIER	33.2°N	126.1°E	72	2003–2011	IM	Gosan, South Korea
WIS	NOAA	31.1°N	34.9°E	400	2000–2011	FM	Negev Desert, Israel
LAN	CAMS	30.3°N	119.7°	139	2009	IM	Lin-an, China
MID	NOAA	28.2°N	177.4°W	4	2000–2011	FM	Midway Island, USA
YON	JMA	24.5°N	123.0°E	30	2000–2011	IM	Yonagunijima, Japan
MNM	JMA	24.3°N	154.0°E	8	2000–2011	IM	Minamitorishima, Japan
HAT	NIES	24.1°N	123.8°E	10	2000–2011	IM	Hateruma, Japan
LLN	NOAA	23.5°N	120.9°E	2867	2006–2011	FM	Lulin, Taiwan
ASK	NOAA	23.2°N	5.4°E	2728	2000–2011	FM	Assekrem, Algeria
MLO	NOAA	19.5°N	155.6°W	3397	2000–2011	FM	Mauna-Loa, Hawaii, USA
GMI	NOAA	13.4°N	144.8°E	2	2000–2011	FM	Mariana Islands, Guam
RPB	AGAGE	13.2°N	59.4°W	3	2000–2011	IM	Ragged Point, Barbados
CHR	NOAA	1.7°N	157.2°W	3	2000–2011	FM	Christmas Island
BKT	NOAA	0.2°S	100.3°E	865	2004–2011	FM	Bukit Kototabang, Indonesia
SMO	AGAGE	14.3°S	170.6°W	42	2000–2011	IM	Tutuila, American Samoa, USA

[a]The altitude indicates the sampling height in meters above sea level.
[b]NOAA flask data were available for 2010-2011 but in situ data from CAMS were only available for 2009.
[c]NOAA flask data were available for 2000–2011, but in situ data from CAMS were only available for 2009.

In situ data were averaged to daily mean values, selecting afternoon values (12:00 to 18:00 LT) for low-altitude sites (to avoid times when there are potentially large errors in the modeled mole fractions from errors in the boundary layer heights) and nighttime values (00:00 to 06:00 LT) for the three mountain sites, KZM, WLG, and LLN, located at 2519, 3816, and 2867 m above sea level, respectively (to avoid times when there might be large errors due to upslope winds, which cannot be resolved at the resolution of the model).

Based on the average repeatability of the measurements, we assumed a constant measurement error of 5 ppb for all observations. We also included an estimate of the uncertainty for how representative the observations are; that is, we used the 1 sigma standard deviation of the observations that were averaged for each daily value. Values for this uncertainty varied considerably from site to site but were in the range of about 1 to 10 ppb. We do not specifically include an estimate for the model transport error, as this is extremely difficult to estimate. Lastly, we included an estimate of the aggregation error (i.e., the error from aggregating the fluxes), which was projected into the observation space, following the method of *Kaminski et al.* [2001]. The total uncertainty in the observation space was calculated as the quadratic sum of all these errors and was used to form the observation error covariance matrix **R**. Since the data used were daytime averages (nighttime averages for mountain sites), the observation errors were assumed to be uncorrelated. However, the aggregation errors are correlated; thus, **R** has off-diagonal elements.

2.5. Atmospheric δ^{13}C-CH_4

Between December 2010 and April 2011, in a proof of concept study, the Royal Holloway University of London (RHUL) took approximately weekly discrete samples for δ^{13}C-CH_4 analysis from a high-rise

Table 2. Prior CH_4 Emission Estimates Shown for 2009

Sources	Reference	Global Total (Tg yr^{-1})
Natural		
Wetlands	*Bergamaschi et al.* [2007]	175
Geological	*Etiope et al.* [2008]	55
Termites	*Sanderson* [1996]	19
Wild animals	*Houweling et al.* [1999]	5
Ocean	*Lambert and Schmidt* [1993]	17
Soil sink	*Ridgwell et al.* [1999]	−38
Anthropogenic		
Rice cultivation[a]	EDGAR-4.2 FT2010	38
Fugitive emissions[b]	EDGAR-4.2 FT2010	118
Fuel combustion[c]	EDGAR-4.2 FT2010	20
Waste[d]	EDGAR-4.2 FT2010	61
Agriculture (nonrice)[e]	EDGAR-4.2 FT2010	113
Biomass burning	GFED-3	13
Total		583

[a]IPCC categories: 4C.
[b]1B1 and 1B2.
[c]1A1 to 1A4 and 7A.
[d]6A, 6B, and 6C.
[e]4A.

waterfront building at about 180 m aboveground level in Kennedy Town, Hong Kong (22.2°N, 114.1°E). In the winter NE monsoon season, the prevailing wind is easterly at around 10 to 12 km h^{-1}. Sea breezes are also easterly, flowing along the harbor [*Liu et al.*, 2001]. Methane $\delta^{13}C$ was analyzed at RHUL using a gas chromatograph isotope ratio mass spectrometer (GC-IRMS, Trace Gas and Isoprime mass spectrometer, Isoprime Ltd.) with a repeatability of 0.05‰ [*Fisher et al.*, 2006]. Retroplumes simulated using FLEXPART show that the Kennedy Town site is well situated for capturing air masses that have passed over eastern China (see section 3). A total of 13 measurements were available. These measurements were complemented by approximately weekly samples at Mount Waliguan, China (36.3°N, 100.9°E), which were used to determine the background. These samples were analyzed for $\delta^{13}C$-CH_4 at the University of Colorado Institute of Arctic and Alpine Research using GC-IRMS (Micromass Optima or Micromass Isoprime mass spectrometer) and have a precision of approximately 0.1‰. Intercomparison between the two laboratories is provided by parallel records at Alert and Ascension. In the inversion, we use the product of the mole fraction and $\delta^{13}C$-CH_4 (see equation (5)), and for this, we chose an uncertainty of 200 (ppb ‰), equivalent to approximately 2.5%.

2.6. Prior Information

Prior estimates for total CH_4 emission (i.e., from all known sources) were compiled from models and inventories for natural and anthropogenic sources (see Table 2). For natural wetland emissions, we used estimates from the Lund-Potsdam-Jena Dynamic Global Vegetation Model, which are provided as a monthly climatology [*Bergamaschi et al.*, 2007]. For ocean emissions, we used the estimate of *Lambert and Schmidt* [1993] provided as an annual climatology. Geological emissions occur from volcanoes and other geothermal activity as well as from marine and land seepage [*Etiope et al.*, 2008]. For these, we used the emission rates of *Etiope* [2009] for geological seeps distributed according to the Global Onshore Gas-Oil Seepage map (http://www.searchanddiscovery.com/documents/2009/090806etiope/). The emissions were then scaled to give a global total of 53 Tg yr^{-1} commensurate with the estimate of *Etiope et al.* [2008]. For termite and wild animal emissions, we used the estimates from *Sanderson* [1996] and *Houweling et al.* [1999], respectively, both annual climatologies. Soil uptake of CH_4 was prescribed by the estimate of *Ridgwell et al.* [1999] provided as a monthly climatology. All these data sets were provided at 1.0° × 1.0° resolution. Anthropogenic emissions (including rice cultivation but excluding biomass burning) were taken from the Emission Database for Global Atmospheric Research (EDGAR-4.2 FT2010, abbreviated from hereon as EDGAR), which are provided annually at 0.1° × 0.1° resolution. Since EDGAR contains no information about the seasonality of the source, which is particularly important for rice cultivation emissions, we applied the seasonality of *Matthews et al.* [1991] to this source type while maintaining the same annual total emission as in EDGAR. Biomass-burning emissions (natural and anthropogenic) were used from the Global Fire Emission Database (GFED-3), which are provided monthly at 0.5°×0.5° resolution. In total, our prior CH_4 emission estimate ranged from 541 to 610 Tg yr^{-1} over 2000–2011 and is broadly consistent with recent global top-down estimates [*Kirschke et al.*, 2013]. For 2011, we used the anthropogenic emissions estimate from 2010 as no value was available from EDGAR for this year.

Table 3. Comparison of TM5 With Observations at Sites Remote from Local Sources

Site ID	Mean Bias (ppb)
ALT	5.6
ASK	0.2
AZR	−2.4
CBA	−4.1
CHR	5.4
COI	1.1
GMI	3.0
HAT	8.4
KZD	−5.7
MHD	7.3
MID	2.0
MLO	6.2
MNM	7.5
SHM	−1.2
SUM	−1.7
THD	2.8
UUM	6.6
WLG	−3.7
YON	3.6
Mean of all sites	2.2

Prior flux uncertainties were determined for each grid cell by taking the maximum flux value of the grid cell of interest plus the eight surrounding ones. This was done to increase the uncertainty for grid cells with only very small prior fluxes, especially where the prior flux pattern is very heterogeneous. Correlations between uncertainties were determined using an exponential decay function with a scale length of 500 km on land and 1000 km over ocean and of 90 days. The spatial correlation length on land was loosely based on the correlation length between ecosystem types but was also a compromise between allowing enough degrees of freedom for the inversion to adjust the spatial pattern of the fluxes and having a well-conditioned matrix for inversion. The full error covariance matrix for the domain, **B**, was found as the Kronecker product of the temporal and spatial covariance matrices. Lastly, the matrix **B** was scaled so that the sum of **B** was equivalent to a total uncertainty of 10 Tg yr^{-1} for the whole East Asian domain.

2.7. Background Mole Fraction Calculation

The background accounts for the mole fraction changes at each observation site that are not accounted for by the transport of CH_4 from fluxes within the domain (shown in Figure 1). There are two components to the background: (1) the initial mole fraction of the retroplume when it terminates 20 days in the past (note that the retroplumes are calculated globally) and (2) the contribution from fluxes outside the domain but within the 20 day retroplume calculation. The initial mole fractions of CH_4 were estimated by coupling FLEXPART retroplumes to global coarse resolution CH_4 simulations from the TM5 chemistry transport model using CH_4 fluxes optimized using NOAA CCGG observations [*Bergamaschi et al*., 2013]. At the termination of the virtual particles (i.e., after 20 days backward in time), FLEXPART calculates the sensitivity at the receptor to the mole fraction at termination (units of ppb ppb^{-1}) in every grid cell. These sensitivity fields were output for 12 vertical layers with layer tops at 100, 500, 1000, 2000, 3000, 5000, 7000, 9000, 12,000, 15,000, 20,000, and 50,000 m above sea level. The initial mole fraction for each retroplume can then be found by multiplying the sensitivity with the 3-D coarse resolution fields of CH_4 mole fraction and integrating the product over the whole globe [*Thompson and Stohl*, 2014]. The initial mole fractions account for spatiotemporal variations due to surface fluxes and chemical reactions occurring further back in time than the 20 days of the FLEXPART retroplumes, projected by FLEXPART onto the observation locations and times. The contribution to the change in mole fraction from fluxes outside the domain was calculated by multiplying the SRRs for outside the domain with the prior flux estimate. This component is added to the initial mole fractions to give the total background for each observation.

Although FLEXINVERT allows for the background to be optimized in the inversion, in this study we chose not to optimize it, as we found that there was insufficient constraint on the background to avoid so-called "cross talk" between the background and the fluxes. However, based on the comparison of the simulated CH_4 mole fraction from TM5 with observations at sites, which were remote from strong emissions (Table 3), we do not consider that there is a significant bias in the background. The mean TM5—observation biases for 2000 to 2011 for the different sites, varied between −5.7 and 8.4 ppb (mean of 2.2 ppb over all sites). Considering that the background is not taken directly from TM5 at each given site, but is calculated by coupling the end points of the FLEXPART trajectories to 3-D concentration fields, the final bias in the background is likely to be closer to the average bias over the northern hemisphere and in the order of the mean bias over all sites.

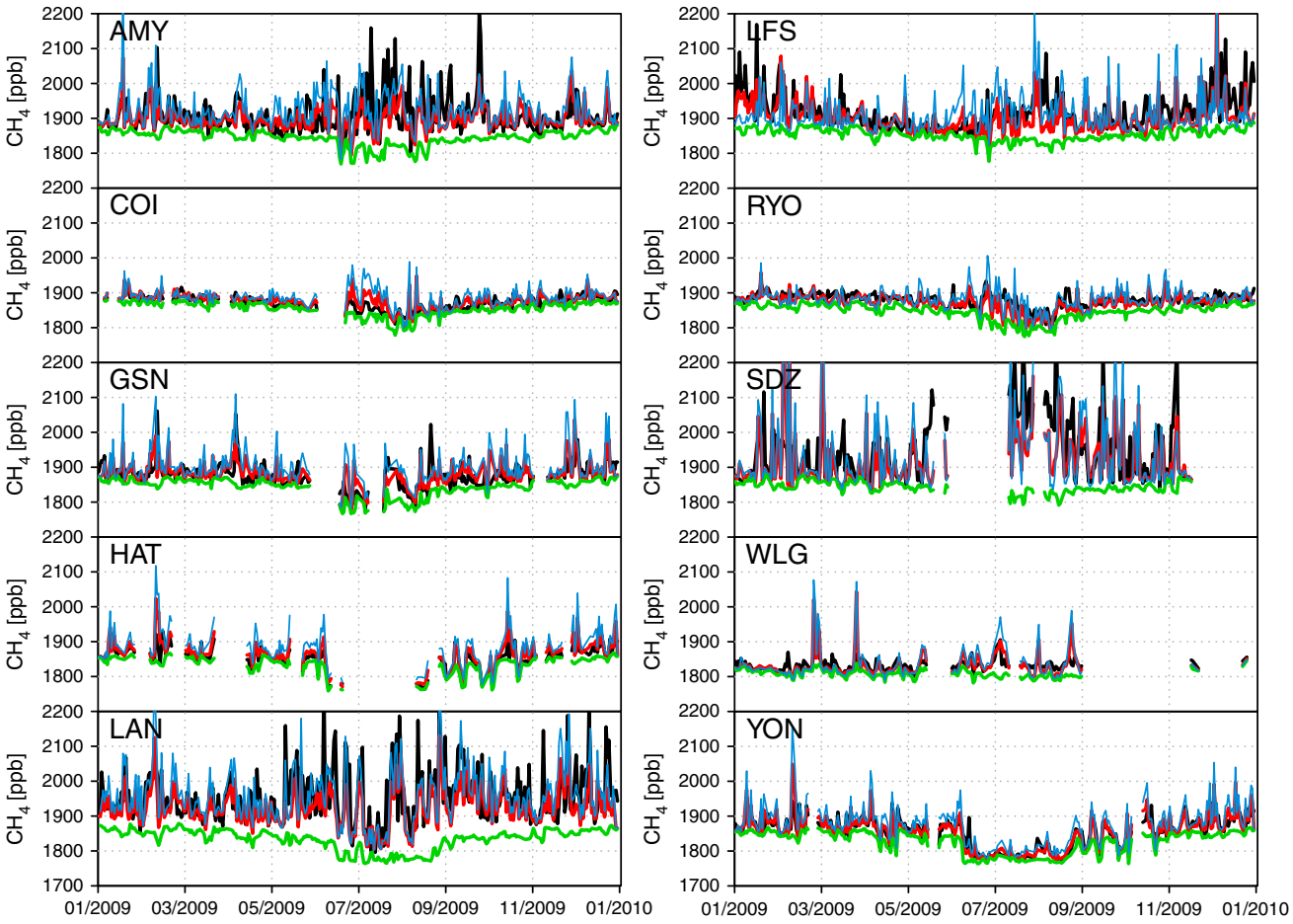

Figure 2. Comparison of atmospheric mole fractions (ppb) at in situ sites in the East Asian domain for 2009. (Legend: prior = blue, posterior = red, background = green, observed = black).

3. Results

3.1. Evaluation of the Inversion

To assess the assumptions made about the uncertainties and error correlation scales used in **B** and **R**, we use the reduced χ^2 statistic, which has the value of the cost function at the optimum (equivalently the weighted sum of squares divided by the number of observations). Ideally, χ^2 would be equal to 1, indicating that the posterior solution is within the limits of the prescribed uncertainties. For each of the 12 month inversions, we find χ^2 values of slightly larger than 1, i.e., between 2.6 and 3.9, indicating that the chosen uncertainty parameters are close to the ideal uncertainties. The number of observations used in each year varied from 2766 in 2000 to 4493 in 2009, when the CAMS data were available.

In all the inversions in this study, we have applied an inequality constraint, i.e., that the fluxes should not be less than zero, as described in section 2.1. Without this constraint, some small areas of negative fluxes (up to $-0.05\,\mathrm{g\,m^{-2}\,d^{-1}}$) appeared in the posterior fluxes and were located in parts of the grid with $1.0° \times 1.0°$ resolution and adjacent to areas with large positive fluxes. This dipolar pattern indicates that there was insufficient information to properly resolve the fluxes at $1.0° \times 1.0°$ resolution in these regions. Applying the inequality constraint brought the negative fluxes to zero (within the range of uncertainty) and effectively smoothed the fluxes in these dipolar regions. The total fluxes for the domain with and without the constraint were similar, within $4\,\mathrm{Tg\,yr^{-1}}$.

Figure 2 shows the comparison of observed versus prior and posterior simulated mole fractions, as well as the background mole fractions, for East Asian sites in 2009. As expected, we find an improved fit to the

Table 4. Comparison of Observed and Simulated CH_4 Mole Fractions (ppb) at Sites Inside the Domain for 2009 When CAMS Data Are Available[a]

	Prior			Posterior		
Site ID	RMSE	R	NSD	RMSE	R	NSD
LFS	61.45	0.37	1.23	46.89	0.54	0.88
SDZ	102.93	0.55	1.12	89.61	0.60	0.88
RYO	24.45	0.55	1.57	18.99	0.52	0.96
AMY	64.81	0.43	0.95	53.60	0.50	0.62
WLG	36.29	0.55	2.49	27.17	0.48	1.82
GSN	49.70	0.45	1.53	33.38	0.44	0.99
YON	36.27	0.63	1.82	21.61	0.62	1.24
MNM	10.60	0.44	1.61	8.24	0.40	1.13
HAT	44.39	0.67	2.13	22.86	0.68	1.41
LAN	67.07	0.60	0.93	65.78	0.64	0.67
KZD	49.21	0.69	1.14	28.53	0.87	1.25
COI	28.94	0.42	2.31	17.11	0.41	1.42
LLN	28.40	0.39	1.31	26.11	0.39	0.93
UUM	85.92	0.24	2.99	62.26	0.22	2.35
KZM	29.56	0.28	0.24	19.68	0.60	0.59
TAP	43.69	0.67	1.57	29.66	0.74	1.08

[a]Shown statistics are the root-mean-square error (RMSE), correlation (*R*), and normalized standard deviation (NSD).

observations in terms of the root-mean-square error (RMSE), normalized standard deviation (NSD), and correlation (*R*) a posteriori compared to a priori (see Table 4). A number of sites (AMY, LAN, LFS, and SDZ) are strongly influenced by local emissions and thus have mole fractions well above the calculated background, while the remaining sites, which are more remote from the emissions, have mixing ratios close to the background. This shows that using a global Eulerian model to define the background mixing ratios can be more reliable than using a statistical baseline extraction method on the observations at each site, which in cases where the sites are strongly influenced by local emissions would lead to an overestimate of the background and, thus, an underestimate of the emissions.

The error reduction, calculated as one minus the ratio of the posterior to prior uncertainty, is a useful indication of how well the fluxes are constrained. Figure 3 shows the annual error reductions for 2007 and 2009. Since the observation sites do not change significantly from 2001 to 2008 and 2010 to 2011, and since the total number of observations is similar, the error reduction for 2007 is representative of the error reductions across all these years. For 2009, the additional observations at the CAMS sites were included; thus, the error reduction is greater in this year. To test the sensitivity of the posterior fluxes to the change in network, notably to the addition of the CAMS sites, we compare fluxes found for 2009 with and without CAMS data (see Figure 4). For East Asia, the two inversions (with and without CAMS) differed by 2.3 Tg yr^{-1} (4%) and for China by 2.5 Tg yr^{-1} (5%). The results for both inversions are similar and show the same location of emission hot spots. In years 2007 and 2009 (years without and with CAMS data, respectively), the largest error reductions (up to 50%) are in the eastern provinces of China and in Japan, while only moderate error reductions are achieved in western China and South Asia (approximately 10%) (Figure 3). This pattern reflects strongly the distribution of the observation sites and, thus, the emission sensitivities. Since the error reduction is small for South Asia, we do not discuss this region further but instead focus on East Asia (i.e., China, Mongolia, North Korea, South Korea, Taiwan, and Japan) in the following sections.

3.2. Total Emissions

Figure 5 shows the mean a posteriori emission and mean increment, i.e., the posterior minus the prior emissions, for 2000 to 2011. Several hot spots were found in the posterior fluxes, which were also present in prior fluxes, specifically in the provinces of Shaanxi, Shanxi, Hebei, and Henan, in central eastern China, as well as in Heilongjiang, in northeastern China. In the prior (i.e., EDGAR), these hot spots are due to emissions related to oil, gas, and/or coal production and transport. Generally, the emissions are higher in eastern China, notably around Beijing and Shanghai, and in the southeast around Hong Kong and Macau.

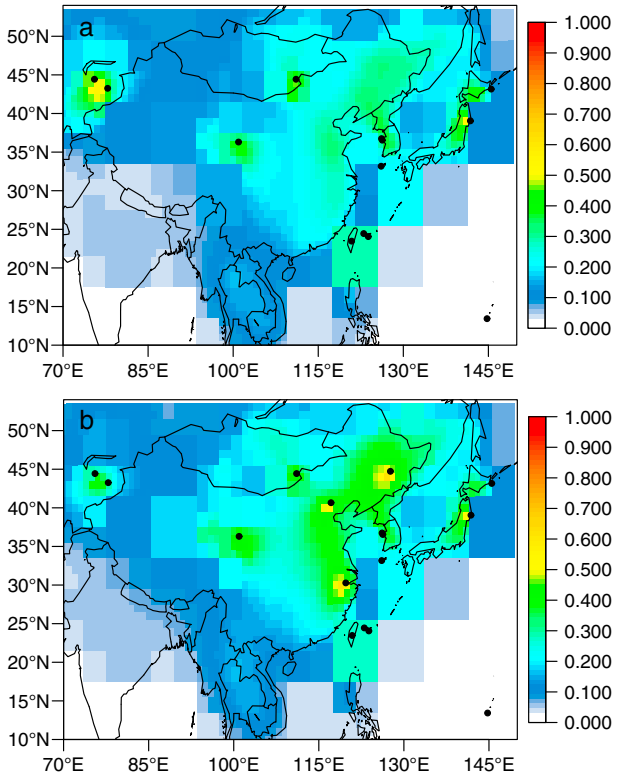

Figure 3. Annual mean relative error reductions (fraction of 1.0) for inversions in (a) 2007 (a year when no CAMS data were available) and (b) 2009 (the year when CAMS data were available). The observation sites are shown by the black dots.

Relative to the prior, the inversion found lower emissions in eastern and southern China and in Japan but slightly higher emissions in Qinghai. In 2009, higher emissions were also found in the provinces of Beijing and Hebei, which are likely owing to the better constraint on emissions in this year (due to the availability of CAMS data) and cannot therefore be ruled out as a possibility in other years too.

For all years, we found lower total emissions from East Asia a posteriori compared to a priori, by 29% on average (Figure 6). This was largely owing to a reduction in emissions from China, which were also found to be 29% lower than in the prior. Emissions from South Korea and Japan were found to be lower than in the prior as well (by 20% and 23%, respectively), but this made only a small difference to the overall East Asian budget, as the South Korean and Japanese emissions are small (total of 2.4 Tg yr^{-1} for the average over 2000–2011) compared to the Chinese emissions (average total of 43.9 Tg yr^{-1}). We do not discuss the national emissions of Mongolia, North Korea, and Taiwan as the total emission for all of these countries is less than 2 Tg yr^{-1} and the relative uncertainty is in the order of 50%; however, these are included in the East Asian total.

We find a significant trend in the emissions from the inversion for East Asia, 1.23 ± 0.18 Tg yr^{-1} ($R^2 = 0.80$), and China, 1.21 ± 0.43 Tg yr^{-1} ($R^2 = 0.88$), over 2000–2011, but no significant trends for the other countries. The trend in East Asia is driven almost entirely by that of China. Figure 7 shows the comparison of the prior and posterior trends for China with the mean emission for 2000–2011 subtracted. The posterior trend is significantly smaller than that of the prior, 2.76 ± 0.59 Tg yr^{-1} ($R^2 = 0.97$), which is largely driven by the increasing coal mining and industrial emissions in the EDGAR data set.

Figure 8 shows CH_4 emissions integrated over East Asia at monthly resolution from 2000 to 2011. The temporal variability in the emissions from China follows the same pattern as for all East Asia and is therefore not shown separately. The emissions show a clear seasonal cycle with a maximum in August, a priori, and in July, a posteriori. In addition, there is a secondary maximum around March, a posteriori. The amplitude of the seasonal cycle found from in the inversion is smaller (16 Tg yr^{-1}) compared to that in the prior (32 Tg yr^{-1}) with the largest difference occurring in summer, i.e., in the maximum.

3.3. Emissions by Source Type

Measurements of CH_4 mole fractions and $\delta^{13}C$-CH_4 from Kennedy Town, Hong Kong (Figure 9), and from Mount Waliguan, China (for winter 2010 to spring 2011), were used to constrain CH_4 emissions by source type in a proof of concept study. The Hong Kong site is well located for observing air masses that pass over eastern China in winter to spring, as shown by the FLEXPART emission sensitivity footprint calculated for the observations (Figure 10), while Mount Waliguan is more representative of the well-mixed troposphere and was therefore used for determining the background.

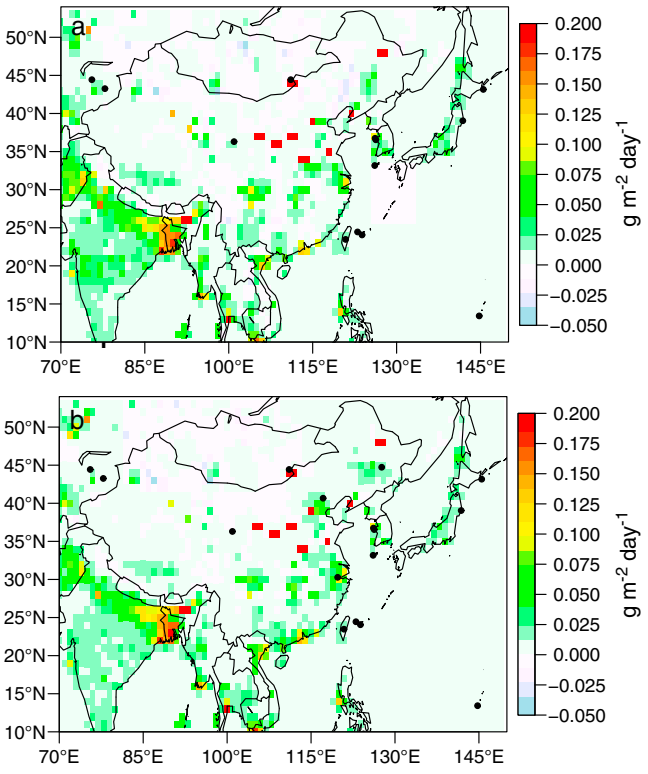

Figure 4. Annual mean posterior CH_4 emissions for 2009 (units of g m^{-2} d^{-1}) determined (a) without CAMS data and (b) with CAMS data. The observation sites are shown by the black dots.

Table 5 shows the contribution by source type a priori and a posteriori to total emissions from China for winter 2010 to spring 2011. The total a priori emission for this period is substantially lower (50.9 ± 3.3 Tg yr^{-1}) than the annual mean (75.2 Tg yr^{-1}) owing largely the difference in rice agriculture emissions, which are at a minimum in the winter and spring. A posteriori, the emission is larger (58.3 ± 3.0 Tg yr^{-1}) and is possibly an overestimate as it is also larger than that found from the inversion using all observation sites for the same period (51.8 ± 3.7 Tg yr^{-1}). The increase in emission a posteriori compared to a priori is due to increases in the landfill and ruminant animal sources; however, both these results were associated with only minor error reductions (26% and 10%, respectively). Although the error reduction is small, this result is relatively robust with respect to the choice of background mole fraction and δ^{13}C-CH_4. We tested the influence of the background by using constant values for the mole fraction and δ^{13}C-CH_4 (of 1857 ppb and −47.3‰, the mean of the Mount Waliguan measurements, respectively). The results were not significantly different to those of the control inversion. Another consideration is the uncertainty in the source signatures used in the inversion. Owing to the limited data available, we allocated the sources to seven categories each with its own source signature, but the signature can vary significantly within each of these categories, which could influence the results. However, until more data are available, it is not possible to adequately account for these variations in the source signatures.

4. Discussion

4.1. Emissions by Region and Source Type

The mean a posteriori CH_4 emission for China for 2000 to 2011 (44 ± 3.5 Tg yr^{-1}) was significantly lower than that a priori (62 ± 6.1 Tg yr^{-1}) but close to top-down estimates from global models for the 2000s (approximately 50 Tg yr^{-1} [*Kirschke et al.*, 2013]). For every year of our inversion, the spatial pattern of emissions was similar, indicating persistent areas of high emissions in eastern China and, especially, in densely populated areas. Also similar for every year was the pattern of emission increments (i.e., posterior minus prior emissions) indicating that the prior persistently overestimates emissions in eastern and southern China. In particular, the largest emission reductions, with respect to the prior, were found in summer and autumn in the provinces of Henan, Hubei, Anhui, Jiangsu, and Zhejiang, in the east, and Hunan, Jiangxi, Guangdong, and Guangxi, in the south. Based on bottom-up estimates, Hunan and Jiangxi are expected to be the two most important provinces for CH_4 emissions from rice cultivation in China, while the other provinces are moderately important [*Chen et al.*, 2013]. On the other hand, these provinces have low emissions from coal mining [*Cheng et al.*, 2011]. Since rice cultivation is an important source for these regions, and considering that the biggest emission reductions are in summer to autumn, when rice emissions are expected to be at a maximum, it is likely that it is the rice cultivation source that is

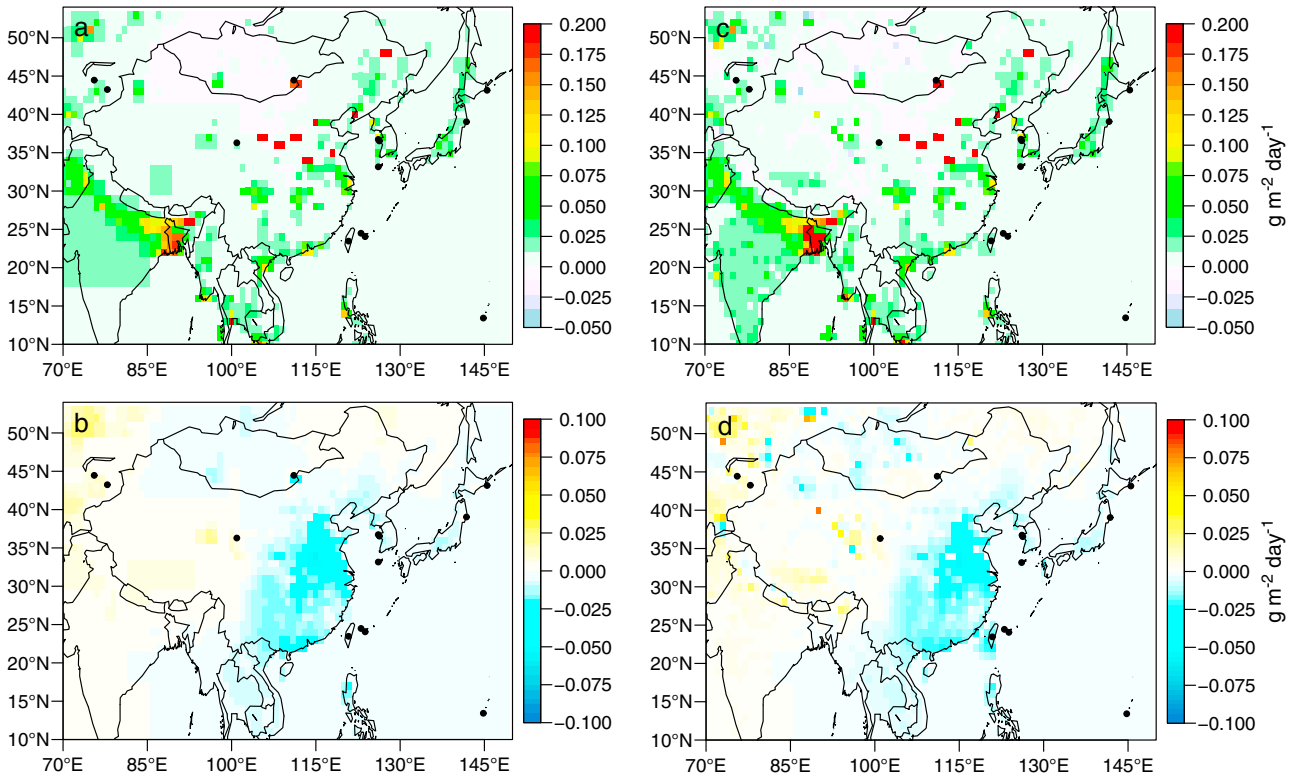

Figure 5. (a) Mean CH_4 emission a posteriori and (b) the difference (a posteriori minus a priori) for the period of 2000 to 2011 shown on the variable grid in units of g m^{-2} d^{-1}. (c) The posterior emissions and (d) difference on the fine grid are also shown. The observation sites are shown by the black dots (excluding the CAMS sites).

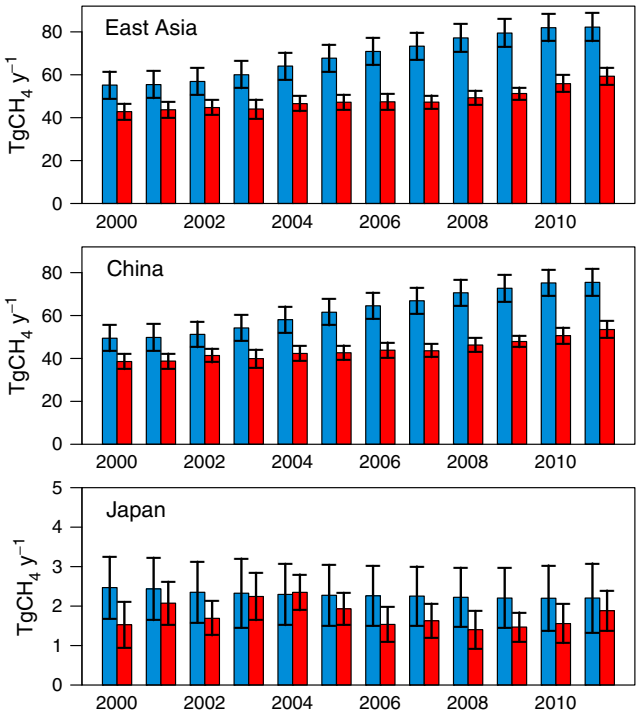

Figure 6. Total annual CH_4 emission a priori (blue) and a posteriori (red) for East Asia, China, and Japan for 2000 to 2011 in units of Tg yr^{-1}. The countries included in East Asia are China, Mongolia, North Korea, South Korea, Taiwan, and Japan. Note that the *y* axis scale for Japan is only 0 to 5 Tg yr^{-1}.

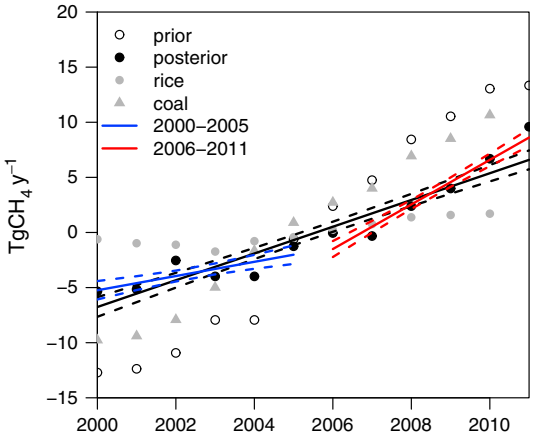

Figure 7. Trends in CH_4 emissions (Tg yr^{-1}) from China for 2000 to 2011 for prior and posterior totals and for the rice cultivation and coal mining emissions from EDGAR-4.2 FT2010. The regressions for the posterior emissions for the period of 2000–2011 (black), 2000–2005 (blue), and 2006–2011 (red) with the 1 sigma confidence intervals indicated by the dashed lines are also shown. Note that the mean emissions for 2000–2011 have been subtracted.

overestimated in EDGAR. Unfortunately, no $\delta^{13}C$-CH_4 measurements were available from Kennedy Town during the summer and autumn, so we cannot verify this with the inversion by source type.

In the EDGAR estimate, Chinese emissions from rice decreased by an average of 0.27 Tg yr^{-1} annually from 1970 to 2003 but increased again by an average of 0.5 Tg yr^{-1} annually from 2003 to 2010. However, there is independent observational evidence that rice agriculture emissions have not increased recently but have in fact continued to decline. The review paper of *Chen et al.* [2013] looked at 412 sets of mean seasonal CH_4 emissions and found that the mean emission rate has declined in the major rice cultivation regions of China from 1987 to 2007, which they attributed to changes in management, such as irrigation and manure input, as well as to a northward migration of rice cultivation, since rice paddies emit less CH_4 in northern regions compared to southern ones. The EDGAR rice cultivation emission of 13.6 Tg yr^{-1} (average 2000–2010) appears to be overestimated compared also to other studies, such as that of *Chen et al.* [2013] who estimated an emission of 8.1 Tg yr^{-1} based on measurements and *Yan et al.* [2009] who estimated an emission of 7.4 Tg yr^{-1} based on the Intergovernmental Panel on Climate Change (IPCC) 2006 Guidelines.

Particularly, high emissions were found a priori and a posteriori in Shanxi, in eastern China, which is the province thought to have the largest emissions of CH_4 from coal mining [*Cheng et al.*, 2011]. High emissions were also found in the provinces of Heilongjiang and Hebei, in northeast and eastern China, respectively, which are also important regions for coal production and, hence, coal mining emissions [*Cheng et al.*, 2011]. For China as a whole, we found 32.0 ± 2.2 Tg yr^{-1} from coal mining and industry in winter 2010 to spring 2011 (based on the inversion of the isotopic data), which was not significantly different from the prior estimate in EDGAR. Our estimate is lower than that of *Zhang and Chen* [2010] of 39.6 Tg yr^{-1} for 2007 but considerably higher than that of *Cheng et al.* [2011] of 13.8 Tg yr^{-1} also for 2007. Considering the total emission from China to be approximately 44 Tg yr^{-1} for 2007 from the inversion, it is unlikely that the coal mining and industrial emission is as low as 13.8 Tg yr^{-1}, since this would require emissions from the other major sources, such as rice cultivation, to be unrealistically high, i.e., equivalent to about 3 times current bottom-up estimates.

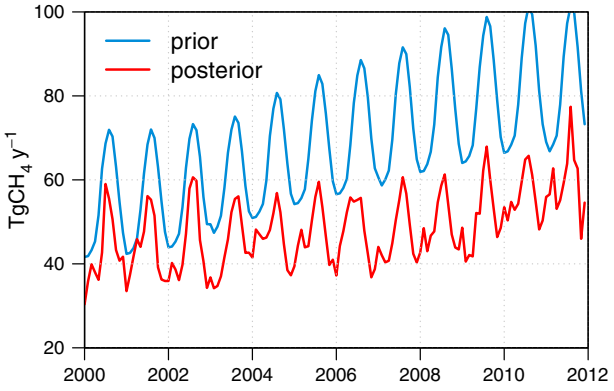

Figure 8. Temporal variability of the total CH_4 emission (Tg yr^{-1}) a priori (blue) and a posteriori (red) from East Asia at monthly resolution for the period of 2000 to 2011.

4.2. Emission Trends

The inversion found a significantly lower trend in emissions for China, of 1.2 ± 0.2 Tg yr^{-1}, than in the prior estimate, 2.8 ± 0.2 Tg yr^{-1}, for the average over 2000–2011 (Figure 7).

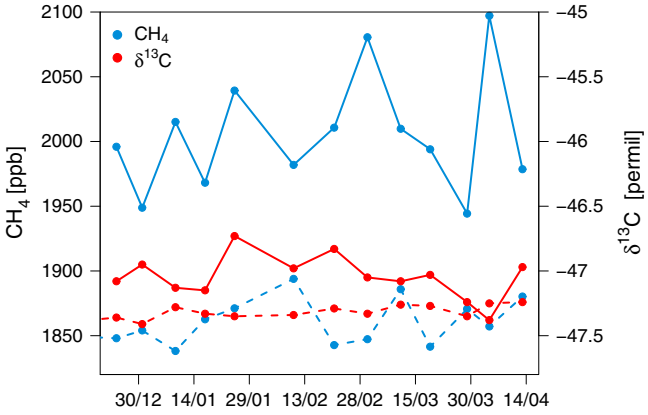

Figure 9. Observations of CH_4 mole fractions (blue) and $\delta^{13}C$-CH_4 (red) at Kennedy Town, Hong Kong (solid lines), and at Mount Waliguan, China (dashed lines), from December 2010 to April 2011.

The strong trend in the prior emissions is largely owing to the anthropogenic emissions in EDGAR. Specifically, EDGAR displays strong trends in emissions from coal mining and industry, of 2.0 Tg yr^{-1} for 2000–2010, and, to a lesser extent, rice cultivation, of 0.5 Tg yr^{-1} for 2003–2010. As discussed above, it is likely that emissions from rice cultivation have declined during the 2000s rather than increased and, from the inversion, emissions only from major rice growing regions in China show no trend over 2000–2011. The emission trend in EDGAR for coal mining and industry is more consistent with that found from the inversion for the period of 2006–2011 of 2.0 ± 1.3 Tg yr^{-1} and is a likely explanation for the trend (see Figure 7). Furthermore, from the inversion, emissions from only the major coal mining regions in China show a trend of 0.70 ± 0.03 Tg yr^{-1} ($R^2 = 0.98$). Coal production increased in China at an average rate of 10% per year throughout the 2000s (according to the BP Statistical Review of World Energy 2010). This rate is higher than that of the CH_4 emission increase over the same period, which we calculate to be approximately 3% per year. However, improvements in mining technology and mitigation policies may mean that the CH_4 emission from coal mining does not necessarily scale one-to-one with coal production [*Cheng et al.*, 2011]. Furthermore, the fact that coal production has been increasing quasiexponentially may explain the appearance of a lower absolute annual CH_4 emission rate for 2000–2005 compared to 2006–2011.

Our results agree well with those of the global inversion of *Bergamaschi et al.* [2013], who found a mean trend for China of 1.1 Tg yr^{-1} over 2000–2010. On one hand, this agreement is not unexpected considering that the background mole fractions for the inversion in this study were from the same inversion model as that used by *Bergamaschi et al.* [2013]. On the other hand, it is reassuring that both the *Bergamaschi et al.* [2013] and our inversion produce consistent results, considering that the transport functions (SRRs) over East Asia are completely independent and are susceptible to different errors depending on, e.g., the transport model and meteorology used, and that our study included East Asian sites not used by *Bergamaschi et al.* [2013].

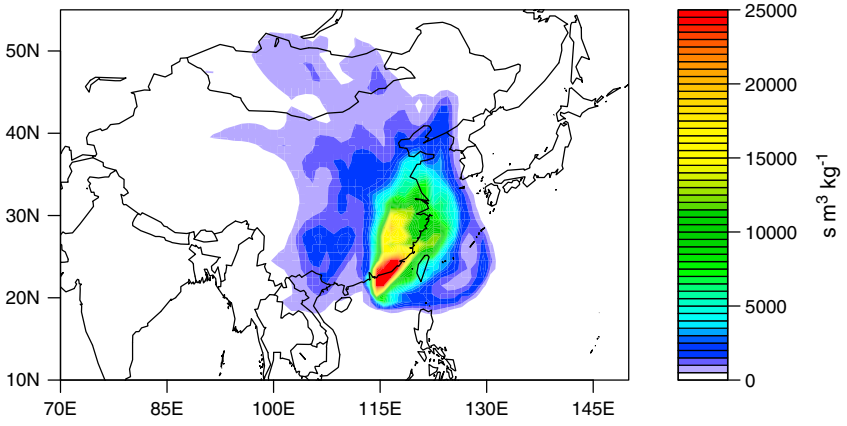

Figure 10. Integrated emission sensitivity footprint for the observations at Kennedy Town, Hong Kong, in units of s m^{-3} kg^{-1}.

Table 5. Contribution of Different CH_4 Sources to Total Chinese Emissions in Winter 2010 to Spring 2011

		Prior		Posterior	
Source Type	$\delta^{13}C$[a]	Tg yr^{-1}	%	Tg yr^{-1}	%
Coal mining and industry[b]	−35‰	30.6 ± 3.1	60	32.0 ± 2.2	55
Rice agriculture[c]	−62‰	2.7 ± 0.3	5	3.2 ± 0.3	5
Wetlands[d]	−55‰	1.0 ± 0.1	2	1.1 ± 0.1	2
Landfills[e]	−53‰	4.1 ± 0.4	8	6.4 ± 0.4	11
Animal waste[f]	−58‰	1.7 ± 0.2	3	1.8 ± 0.2	3
Ruminant animals[g]	−60‰	10.7 ± 1.1	21	13.7 ± 1.2	23
Biomass burning[h] (C3)	−26‰	0.1 ± 0.01	0.2	0.1 ± 0.01	0.2
Total		50.9		58.3	

[a]Isotopic values are taken from *Dlugokencky et al.* [2011], and references therein.
[b]IPCC categories: 1A1, 1A2, 1B1, 1B2, and 7A.
[c]4C.
[d]*Bergamaschi et al.*, [2007].
[e]6A and 6C.
[f]4B.
[g]4A.
[h]GFED-3.

Bergamaschi et al. [2013] find a significant increase, of 16–20 Tg yr^{-1}, in the global emissions in 2007–2010 relative to 2003–2005, of which they attribute approximately 60% to changes in tropical emissions and 40% to changes in Northern Hemisphere (NH) extratropical emissions. This NH extratropical contribution to the global change, 6–8 Tg yr^{-1}, is likely to be driven by emissions from China, for which we find a difference of 6 Tg yr^{-1} for the 2007–2010 versus 2003–2005 emissions (see also Table 6).

4.3. Comparison to Other Regional Top-Down Estimates

We compare our inversion estimates for the total CH_4 emission in East Asia to the regional top-down estimates of *Wada et al.* [2013], based on the radon tracer method, and *Tohjima et al.* [2014], based on CH_4 to CO_2 ratios. *Tohjima et al.* [2014] estimate the nonseasonal component of the emissions, i.e., excluding wetlands and rice cultivation, to be 46 ± 8 Tg yr^{-1} for northern and eastern China in 2009 and 2010. Assuming that the bottom-up estimates for rice and wetland emissions are in the order of 8 and 2 Tg yr^{-1}, respectively, then the total from *Tohjima et al.* [2014] is consistent within the range of uncertainty with our estimate of 49 ± 3 Tg yr^{-1}. *Wada et al.* [2013] estimate the total CH_4 emission, for a catchment area that includes northern and southern China, Korea, and Japan, to be 30 ± 10 Tg yr^{-1} for 2007. This is considerably lower than our estimate for East Asia, of 47 ± 3 Tg yr^{-1} for the same year. The emissions from western China are low and cannot explain the difference between the two estimates. Rather, the difference is likely owing in part to the selection of mole fraction and radon enhancements above the background, which meant that only data from December to April were included [*Wada et al.*, 2013]; thus, their estimate is more valid as an estimate of the winter to spring emissions only and as such, are more consistent, within the range of uncertainty, with our estimate of the 2007 emissions for January to April of 42 ± 3 Tg yr^{-1}.

Table 6. Mean CH_4 Emissions (Tg yr^{-1}) at the National Level for the Periods of 2000–2005 and 2006–2011[a]

	Prior				Posterior			
	China	Japan	South Korea	Other	China	Japan	South Korea	Other
2000–2005	53.4	2.4	0.8	2.6	40.2	2.0	0.7	1.5
2006–2011	70.9	2.2	0.9	3.5	47.6	1.6	0.7	2.0
Uncertainty	6.1	0.8	0.6	1.5	3.5	0.5	0.3	0.8

[a]The category "Other" is for North Korea, Taiwan, and Mongolia.

5. Summary and Conclusions

We have estimated CH_4 emissions from East Asia for 2000–2011 using a Bayesian inversion approach. The total emission for East Asia increased from $43 \pm 4\,Tg\,yr^{-1}$ to $59 \pm 4\,Tg\,yr^{-1}$, while that for China increased from $39 \pm 4\,Tg\,yr^{-1}$ to $54 \pm 4\,Tg\,yr^{-1}$ from 2000 to 2011. For Japan and South Korea, the mean emissions were $0.7 \pm 0.3\,Tg\,yr^{-1}$ and $1.8 \pm 0.5\,Tg\,yr^{-1}$, respectively, and did not display any significant trends. Emissions from Mongolia, North Korea, and Taiwan together totaled $1.7 \pm 0.6\,Tg\,yr^{-1}$ and, likewise, did not display any detectable trend. Compared to the prior estimate, the emissions were significantly lower in China, Japan, and South Korea by 29%, 23%, and 20%, respectively, for the average over 2000–2011. The greatest difference in emissions, a posteriori with respect to a priori, was found in eastern China, especially in regions important for rice agriculture and, in particular, in the summer months. This suggests that it is largely the rice emissions in EDGAR-4.2 FT2010 that are overestimated in the prior.

The largest emissions in East Asia were found in eastern China, with hot spots in the provinces of Shaanxi, Shanxi, Hebei, Henan, and Heilongjiang, as well as high emissions around Beijing, Shanghai, Hong Kong, and Macau. High emissions were also found in Japan. Shanxi, Hebei, and Heilongjiang provinces are important regions for coal mining. Based on our methane isotope inversion for source types (winter 2010 to spring 2011 only), we estimate total coal mining emissions to be $32 \pm 2\,Tg\,yr^{-1}$, which was not significantly different from the prior estimate. Moreover, we found larger landfill and ruminant animal emissions compared to EDGAR-4.2 FT2010, by 56% and 28%, respectively; however, this result is not well constrained owing to the limited number of isotope observations and to the uncertainty in the source signatures.

We found a significant trend in emissions from China of $3.0 \pm 1.0\%$/yr over 2000–2011, which was substantially smaller than that in the prior estimate, of $4.5 \pm 1.0\%$. The trend is likely driven by increases in coal production, which increased at a rate of 10%/yr throughout the 2000s. The trend in Chinese emissions amounts to a difference in the mean emission of $6\,Tg\,yr^{-1}$ for 2007–2010 versus 2003–2005 and explains approximately 40% of the global increase in emissions for these time periods.

Moreover, we found that the four new in situ sites operated by CAMS make a significant contribution to the constraint of emissions in East Asia and improved the error reduction for East Asia in 2009 by 15%, based on the comparison of inversions for 2009 with and without the CAMS data. Similarly, the trial $\delta^{13}C$-CH_4 and CH_4 mole fraction measurements from Kennedy Town offer a strong potential to constrain the emission sources from China, and our analysis of these data was only limited by the small number of observations available.

Acknowledgments

We thank P. Bergamaschi for the use of the TM5 model output (available on request to P. Bergamaschi). In addition, we thank G. van der Werf for the use the GFED data (http://www.globalfiredata.org) and G. Zhao at the University of Hong Kong for collecting the samples for $\delta^{13}C$-CH_4 analysis. The EDGAR-4.2 FT2010 data are available via the EDGAR website (http://edgar.jrc.ec.europa.eu). Atmospheric observations used in this paper are available via the World Data Centre for Greenhouse Gases (http://ds.data.jma.go.jp/gmd/wdcgg/), the NOAA GMD ftp server (http://www.esrl.noaa.gov/gmd/), for the CAMS data, by request to L. Zhou, and for the Kennedy Town methane isotope ratios, by request to E.G. Nisbet. AGAGE is supported principally by NASA (USA) grants to MIT and SIO and by DEFRA (UK) and NOAA (USA) grants to Bristol University, CSIRO and BoM (Australia), Empa (Switzerland), NILU (Norway), SNU (Korea), CMA (China), NIES (Japan), and Urbino University (Italy). We acknowledge the Norwegian Research Council for funding this research in the framework of the SOGG-EA project.

References

Bergamaschi, P., et al. (2007), Satellite chartography of atmospheric methane from SCIAMACHY on board ENVISAT: 2. Evaluation based on inverse model simulations, *J. Geophys. Res.*, *112*, D02304, doi:10.1029/2006JD007268.

Bergamaschi, P., et al. (2009), Inverse modeling of global and regional CH_4 emissions using SCIAMACHY satellite retrievals, *J. Geophys. Res.*, *114*, D22301, doi:10.1029/2009JD012287.

Bergamaschi, P., et al. (2013), Atmospheric CH_4 in the first decade of the 21st century: Inverse modeling analysis using SCIAMACHY satellite retrievals and NOAA surface measurements, *J. Geophys. Res. Atmos.*, *118*, 7350–7369, doi:10.1002/jgrd.50480.

Chen, H., et al. (2013), Methane emissions from rice paddies natural wetlands, lakes in China: Synthesis new estimate, *Global Change Biol.*, *19*(1), 19–32, doi:10.1111/gcb.12034.

Chen, Y.-H., and R. G. Prinn (2006), Estimation of atmospheric methane emissions between 1996 and 2001 using a three-dimensional global chemical transport model, *J. Geophys. Res.*, *111*, D10307, doi:10.1029/2005JD006058.

Cheng, Y.-P., L. Wang, and X.-L. Zhang (2011), Environmental impact of coal mine methane emissions and responding strategies in China, *Int. J. Greenhouse Gas Control*, *5*(1), 157–166, doi:10.1016/j.ijggc.2010.07.007.

Cunnold, D. M., L. P. Steele, P. J. Fraser, P. G. Simmonds, R. G. Prinn, R. F. Weiss, L. W. Porter, S. O'Doherty, R. L. Langenfelds, and P. B. Krummel (2002), In situ measurements of atmospheric methane at GAGE/AGAGE sites during 1985–2000 and resulting source inferences, *J. Geophys. Res.*, *107*(D14), 4225, doi:10.1029/2001JD001226.

Dlugokencky, E. J., R. C. Myers, P. M. Lang, K. A. Masarie, A. M. Crotwell, K. W. Thoning, B. D. Hall, J. W. Elkins, and L. P. Steele (2005), Conversion of NOAA atmospheric dry air CH_4 mole fractions to a gravimetrically prepared standard scale, *J. Geophys. Res.*, *110*, D18306, doi:10.1029/2005JD006035.

Dlugokencky, E. J., E. G. Nisbet, R. Fisher, and D. Lowry (2011), Global atmospheric methane: Budget, changes and dangers, *Philos. Trans. R. Soc. London, Ser. A*, *369*(1943), 2058–2072, doi:10.1098/rsta.2010.0341.

Etiope, G. (2009), Natural emissions of methane from geological seepage in Europe, *Atmos. Environ.*, *43*(7), 1430–1443, doi:10.1016/j.atmosenv.2008.03.014.

Etiope, G., K. R. Lassey, R. W. Klusman, and E. Boschi (2008), Reappraisal of the fossil methane budget and related emission from geologic sources, *Geophys. Res. Lett.*, *35*, L09307, doi:10.1029/2008GL033623.

Fang, S.-X., L.-X. Zhou, K. A. Masarie, L. Xu, and C. W. Rella (2013), Study of atmospheric CH_4 mole fractions at three WMO/GAW stations in China, *J. Geophys. Res. Atmos.*, *118*, 4874–4886, doi:10.1002/jgrd.50284.

Fisher, R., D. Lowry, O. Wilkin, S. Sriskantharajah, and E. G. Nisbet (2006), High-precision, automated stable isotope analysis of atmospheric methane and carbon dioxide using continuous-flow isotope-ratio mass spectrometry, *Rapid Commun. Mass Spectrom.*, *20*(2), 200–208, doi:10.1002/rcm.2300.

Gregg, J. S., R. J. Andres, and G. Marland (2008), China: Emissions pattern of the world leader in CO_2 emissions from fossil fuel consumption and cement production, *Geophys. Res. Lett.*, *35*, L08806, doi:10.1029/2007GL032887.

Houweling, S., T. Kaminski, F. Dentener, J. Lelieveld, and M. Heimann (1999), Inverse modeling of methane sources and sinks using the adjoint of a global transport model, *J. Geophys. Res.*, *104*(D21), 26,137–26,160, doi:10.1029/1999JD900428.

Kaminski, T., P. J. Rayner, M. Heimann, and I. G. Enting (2001), On aggregation errors in atmospheric transport inversions, *J. Geophys. Res.*, *106*(D5), 4703–4715, doi:10.1029/2000JD900581.

Kirschke, S., et al. (2013), Three decades of global methane sources and sinks, *Nat. Geosci.*, *6*(10), 813–823, doi:10.1038/ngeo1955.

Lambert, G., and S. Schmidt (1993), Reevaluation of the oceanic flux of methane: Uncertainties and long term variations, *Chemosphere*, *26*(1), 579–589, doi:10.1016/0045-6535(93)90443-9.

Liu, H., J. C. Chan, and A. Cheng (2001), Internal boundary layer structure under sea-breeze conditions in Hong Kong, *Atmos. Environ.*, *35*(4), 683–692.

Matthews, E., I. Fung, and J. Lerner (1991), Methane emission from rice cultivation: Geographic and seasonal distribution of cultivated areas and emissions, *Global Biogeochem. Cycles*, *5*(1), 3–24, doi:10.1029/90GB02311.

Mikaloff Fletcher, S. E., P. P. Tans, L. M. Bruhwiler, J. B. Miller, and M. Heimann (2004), CH4sources estimated from atmospheric observations of CH4 and its $^{13}C/^{12}C$ isotopic ratios: 1. Inverse modeling of source processes, *Global Biogeochem. Cycles*, *18*, GB4004, doi:10.1029/2004GB002223.

Myhre, G., et al. (2013), Chapter 8: Anthropogenic and natural radiative forcing, in *Climate Change 2013: The Physical Science Basis. Contribution of Working Group I to the Fifth Assessment Report of the Intergovernmental Panel on Climate Change*, edited by T. F. Stocker et al., Cambridge Univ. Press, Cambridge, U. K., and New York

Nisbet, E. G., E. J. Dlugokencky, and P. Bousquet (2014), Methane on the rise—Again, *Science*, *343*(6170), 493–495, doi:10.1126/science.1247828.

Ridgwell, A. J., S. J. Marshall, and K. Gregson (1999), Consumption of atmospheric methane by soils: A process-based model, *Global Biogeochem. Cycles*, *13*(1), 59–70, doi:10.1029/1998GB900004.

Rigby, M., et al. (2008), Renewed growth of atmospheric methane, *Geophys. Res. Lett.*, *35*, L22805, doi:10.1029/2008GL036037.

Sanderson, M. G. (1996), Biomass of termites and their emissions of methane and carbon dioxide: A global database, *Global Biogeochem. Cycles*, *10*(4), 543–557, doi:10.1029/96GB01893.

Seibert, P., and A. Frank (2004), Source-receptor matrix calculation with a Lagrangian particle dispersion model in backward mode, *Atmos. Chem. Phys.*, *4*(1), 51–63, doi:10.5194/acp-4-51-2004.

Stohl, A., M. Hittenberger, and G. Wotawa (1998), Validation of the Lagrangian particle dispersion model FLEXPART against large-scale tracer experiment data, *Atmos. Environ.*, *32*(24), 4245–4264.

Stohl, A., C. Forster, A. Frank, P. Seibert, and G. Wotawa (2005), Technical note: The Lagrangian particle dispersion model FLEXPART version 6.2, *Atmos. Chem. Phys.*, *5*(9), 2461–2474, doi:10.5194/acp-5-2461-2005.

Stohl, A., et al. (2010), Hydrochlorofluorocarbon and hydrofluorocarbon emissions in East Asia determined by inverse modeling, *Atmos. Chem. Phys.*, *10*(8), 3545–3560, doi:10.5194/acp-10-3545-2010.

Tarantola, A. (2005), *Inverse Problem Theory and Methods for Model Parameter Estimation*, pp. 358, Society for Industrial and Applied Mathematics, Philadelphia, Pa.

Thacker, W. C. (2007), Data assimilation with inequality constraints, *Ocean Model.*, *16*(3–4), 264–276, doi:10.1016/j.ocemod.2006.11.001.

Thompson, R. L., and A. Stohl (2014), FLEXINVERT: An atmospheric Bayesian inversion framework for determining surface fluxes of trace species using an optimized grid, *Geosci. Model Dev.*, *7*, 2223–2242, doi:10.5194/gmd-7-2223-2014.

Tohjima, Y., M. Kubo, C. Minejima, H. Mukai, H. Tanimoto, A. Ganshin, S. Maksyutov, K. Katsumata, T. Machida, and K. Kita (2014), Temporal changes in the emissions of CH_4 and CO from China estimated from CH_4/CO_2 and CO/CO_2 correlations observed at Hateruma Island, *Atmos. Chem. Phys.*, *14*(3), 1663–1677, doi:10.5194/acp-14-1663-2014.

Wada, A., H. Matsueda, S. Murayama, S. Taguchi, S. Hirao, H. Yamazawa, J. Moriizumi, K. Tsuboi, Y. Niwa, and Y. Sawa (2013), Quantification of emission estimates of CO_2, CH_4 and CO for East Asia derived from atmospheric radon-222 measurements over the western North Pacific, *Tellus*, *65*, 18,037, doi:10.3402/tellusb.v65i0.18037.

Weiss, R. F., and R. G. Prinn (2011), Quantifying greenhouse-gas emissions from atmospheric measurements: A critical reality check for climate legislation, *Philos. Trans. R. Soc. London, Ser. A*, *369*(1943), 1925–1942, doi:10.1098/rsta.2011.0006.

Yan, X., H. Akiyama, K. Yagi, and H. Akimoto (2009), Global estimations of the inventory and mitigation potential of methane emissions from rice cultivation conducted using the 2006 Intergovernmental Panel on Climate Change Guidelines, *Global Biogeochem. Cycles*, *23*, GB2002, doi:10.1029/2008GB003299.

Zhang, B., and G. Q. Chen (2010), Methane emissions by Chinese economy: Inventory and embodiment analysis, *Energy Policy*, *38*(8), 4304–4316, doi:10.1016/j.enpol.2010.03.059.